SELF-CLEANING MATERIALS—LOTUS EFFECT SURFACES

1. Introduction

The phenomenon of the water repellency of lotus plants has been noticed for a long time, but the surface structure of lotus leaves and its effect on the observed phenomena was not discovered until 1997 when Professor Wilhelm Barthlott (1) from the University of Bonn investigated the self-cleaning property of lotus leaves and discovered the link between their surface appearance and functionalities. It was found that lotus leaves are covered with an array of tiny bumps of 5–10 μm high and 10–15 μm apart, as shown in Figure 1. This uneven surface is covered with waxy crystals in nanometer diameter. He named this kind of phenomenon the "lotus effect", and was the first to examine it for technical applications. However, it is important to note that although called the lotus effect, a wide variety of other plants have similar superhydrophobic and self-cleaning surfaces with different surfaces patterns.

The lotus effect implies two indispensable characteristics: superhydrophobicity and self-cleaning. Superhydrophobicity is often manifested by a water contact angle larger than 150°, while self-cleaning indicates that particles of dirt such as dust or soot are picked up and removed by water drops as they roll off the surface. The superhydrophobicity and self-cleaning property of lotus leaves can be demonstrated by Figure 2. In general, lotus effect surfaces arise when both of the following are achieved: (1) surface is covered with low surface energy materials, such as waxy crystals; (2) surface has a very fine structure. Air can be trapped in the fine structures, and reduces the contact area between the water droplet and solid surface. The actual contact area of the lotus plant leaves is only 2–3% of the water droplet covered surface. Since the 1990s, lotus effect materials replicating superhydrophobicity and self-cleaning of nature lotus leaves on artificial surfaces have gained great attention. Many theoretical studies, processing methods, and new applications of lotus effect materials appear every year. In this article, the relationship between lotus effect, superhydrophobicity, and self-cleaning is discussed. Some theoretical studies on the wettability of a hydrophobic rough surface are introduced, and the processing of lotus effect materials is also summarized. Based on the properties of lotus effect surfaces, different applications are introduced and proposed.

2. Lotus Effect and Superhydrophobicity

As indicated by Nun and co-workers (2), there are no ASTM or ISO standards to characterize lotus effect surfaces. Practically, several analytical parameters can be used to determine if a solid surface is a lotus effect surface. First, the surface must have a large water contact angle (above 150°); second, the *water contact angle* hysterisis, which is defined as the difference between the advancing and receding angles, should be less than 10°; third, the roll off angle, which is also called the sliding angle, should be less than 10°.

The lotus effect implies the superhydrophobicity and the self-cleaning properties of a surface. Today, these three terms, lotus effect, superhydrophobicity, and self-cleaning, are used synonymously in some literatures. Superhydrophobic surfaces with large water contact angle above 150° have been prepared in various experiments since the 1950s (3,4), especially through the plasma processing of polymer materials. However, as indicated by Youngblood and McCarthy (5), it is common that a surface with a large water contact angle may exhibit a large contact angle hysterisis or sliding angle. Water droplets may remain pinned to the surface and show poor water repellency, and dust particles cannot be removed by rolling water droplets. Such kind of surfaces should not be called self-cleaning surfaces. On the other hand, superhydrophilic surfaces (with water contact angle close to 0°) are also called self-cleaning surfaces, because water can spread out on such surfaces and forms a thin film that washes away loose dust particles.

In fact, more and more literature suggest that the concept of superhydrophobicity should include both a large water contact angle and small contact angle hysterisis (5–14), which is also the criterion of forming a lotus effect surface. On such a hydrophobic surface, a water droplet can roll off the surface with a small tilt angle and pick up dust particles, because the adhesion of dust particles is also reduced. Although the lotus effect term was first introduced in 1997, we would like to include earlier superhydrophobic surfaces which also have small contact angle hysterisis in this article (3–78).

3. Effect of Surface Structure on Superhydrophobicity

The influence of roughness on water repellency was studied long before the appearance of the lotus effect term and can be understood on a sound thermodynamic basis.

The wetting of a solid with water, with air as the surrounding medium, is dependent on the relationship between the interfacial tensions of water/air, water/solid, and solid/air. The ratio between these tensions determines the contact angle of a water droplet on a given surface and is described by the Young's equation (eq. 1). If a droplet is applied to a solid surface, it will wet the surface to a certain degree. The wetting depends on the ratio between the energy necessary for the enlargement of the surface and the gain of energy due to adsorption. At equilibrium, the energy of the system is minimized.

$$\cos\theta_Y = \frac{\gamma_{SV} - \gamma_{SL}}{\gamma_{LV}} \tag{1}$$

where θ_Y is called the Young's contact angle, γ_{SL}, γ_{SV}, and γ_{LV} are the interfacial energies per unit area of the solid–liquid (SL), solid–vapor (SV), and liquid–vapor (LV) interfaces, respectively as shown in Figure 3**a**. According to Young's equation, the maximum contact angle can be attained by lowering the surface energy of a flat surface.

The Young's equation can only be applied to a smooth and homogeneous surface. Wetting on rough surfaces has been studied extensively (79–91). Wenzel

recognized (79) that Young's equation does not represent the physical interaction between a rough solid surface and liquid drop. He indicated that the roughness of the surface, and therefore the actual surface area, affects the surface-wetting properties. He modified Young's equation as follows:

$$\cos\theta_{\mathrm{W}} = r\frac{\gamma_{\mathrm{SV}} - \gamma_{\mathrm{SL}}}{\gamma_{\mathrm{LV}}} = r\cos\theta_{\mathrm{Y}} \tag{2}$$

In equation (2), θ_{W} is called the Wenzel contact angle, r is the *roughness factor*, which is defined as the ratio of the actual area of a rough surface to the geometric projected area. Since r is always larger than 1, when the surface roughness increases, the hydrophilicity for hydrophilic surface $(0 < \theta_{\mathrm{Y}} < \pi/2)$ increases and the hydrophobicity for hydrophobic surface $(\pi/2 < \theta_{\mathrm{Y}} < \pi)$ increases. The scenario of Wenzel's equation is called homogeneous wetting and is described in Figure 3**b**. However, note that the Wenzel's equation can only be applied to homogenous rough surfaces.

It is generally understood that when a water drop is placed on a lotus plant leaf surface, the air entrapped in the surface structures prevents the total wetting of the surface, as such only a small part of the surface, such as the tip of the nanostructures, can be in contact with the water drop. Air is enclosed between the wax crystalloids, forming a composite or heterogeneous surface. This enlarges the water/air interface, while the solid/water interface is minimized. Therefore, the water drop gains very little energy through adsorption to compensate for any enlargement of its surface. In this situation, water spreading does not occur; instead the water forms a spherical droplet, the contact angle of which depends almost entirely on the surface tension of the water. The contact angle θ_{C} at a heterogeneous surface can be described by Cassie–Baxter equation (80) as follows:

$$\cos\theta_C = f\cos\theta_{\mathrm{Y}} + f - 1 \tag{3}$$

where f is the remaining area fraction of the liquid–solid interface. According to Cassie–Baxter equation, when f decreases, the water contact angle of a hydrophobic surface will increase. Besides f, the roughness ratio of the surface also affects the wetting properties of a heterogeneous rough surface (13). Therefore, Cassie–Baxter equation can be modified as

$$\cos\theta_C = \Gamma f\cos\theta + f - 1 \tag{4}$$

where Γ is the roughness factor of the wet area. The heterogeneous wetting phenomenon, described by Cassie's equation, is illustrated in Figure 3**c**.

Wenzel and Cassie–Baxter's works laid out the fundamentals of wetting behavior on a hydrophobic rough surface. Based on those works, various theories were proposed and reported with consideration of the effect of gravity, contact line-tension, and three-dimensional structure of surfaces. Johnson and Dettre (92) simulated the contact angle of a water droplet on a sinusoidal surface. They demonstrated that for a hydrophobic surface, water contact angle and its

hysterisis increase with surface roughness, which indicates a Wenzel's region. When the surface roughness factor exceeds a certain value, the contact angle hysterisis decreases and Cassie–Baxter contact angle becomes the preferred equilibrium state. Marmur (13) extended this work. With thermodynamic perspective, he defined the conditions for determining the transition between the Wenzel and Cassie–Baxter's wetting regimes for some simple rough surfaces, which included surface with semicircular protrusions, surface with circular protrusions, saw-toothed surface, and surface with semicircular grooves.

In addition, Drelich and Miller (90) derived a modification of the Cassie equation on the basis of the generalized Young equation including the line-tension term. They then applied the modified Cassie–Baxter equation for the interpretation of contact angle data reported for heterogeneous surfaces. Wolansky and Marmur (89) presented a general equation for the actual contact angle on a solid surface in a three-dimensional setting. The effect of line tension and the contact line position were considered. By using the long-range noise correlation function, Chow (84) described the wetting phenomena and the contact line depinning as a function of the microstructure of rough surfaces, and indicated that roughness enhances wetting and broadens the three-phase contact line. Using a minimization technique on the free energy of this system, Swain and Lipowsky (93) derived a generalized Young's equation for the contact angle of liquid drop sitting on a rough and chemically heterogeneous substrate while keeping account of gravity and line tension terms. Feng and co-workers (22) used the fractal formula to calculate the roughness factor of a lotus leaf, and determined the water contact angle on such a surface with Cassie's equation. Oner and McCarthy (9) studied the wettability of a series of silicon surfaces that were prepared by photolithography and hydrophobized with silanization reagents. It is indicated that the contact length decrease and the three-phase contact line tortuosity increase can enhance surface hydrophobicity and reduce contact angle hysterisis. Extrand (12) proposed a criterion based on contact line density for predicting the condition that produce superhydrophobic surfaces. The criterion value of the contact line density was determined by contact angle, asperity shape, and properties of the contact liquid. Generally, superhydrophobicity can be obtained on a rough hydrophobic surface if air bubbles can be trapped in a proper-shaped surface structure. It is also observed that with air entrapped, hydrophilic surface can be made superhydrophobic, but this state is only metastable, because a hydrophilic surface gains energy by being covered with liquid. Based on this observation, Bico and co-workers (94) indicated that the solid must be hydrophobic enough for air trapping to be stable, which is consistent with the Cassie–Baxter equation.

4. Contact Angle Hysterisis

As mentioned early in the Introduction, a high static water contact angle is not sufficient to describe a lotus effect surface. Chen and co-workers (7) indicated that contact angle hysterisis is more important in characterizing superhydrophobicity than the maximum achievable contact angle. In addition, the self-cleaning requires both low adhesion between dust particles and the surface and rolling water

droplets to overcome this adhesion and its ability to pick up these particles from the surface. When a water droplet has both a high contact angle and low contact angle hysterisis, it can easily roll off the surface with a slight tilt of the surface.

The effect of surface roughness and surface composition on a stable equilibrium contact angle can be described by Wenzel or Cassie–Baxter equation. Similar to the stable equilibrium contact angle, contact angle hysterisis also depends on surface roughness and surface composition, both of which introduce many closely spaced metastable states, which may be in metastable equilibrium.

The relationship between sliding angle or contact angle hysterisis and surface wetting properties was noticed a long time ago (95,96). The empirical relationship between sliding angle α and drop size is

$$\sin \alpha = k\frac{2r\pi}{mg} \tag{5}$$

where mg is the drop weight and r is the radius of the wetted area. The constant k can be correlated with surface tension, contact angle, and surface roughness. The relationship between sliding angle and contact angle hysterisis is proposed by Furmidge (95):

$$mg \sin\alpha \approx \gamma_{\mathrm{LV}}(\cos\theta_{\mathrm{R}} - \cos\theta_{\mathrm{A}})w \tag{6}$$

where $w = 2r$ and γ_{LV} is the liquid–vapor surface tension. The sliding angle and contact angle of water droplet on a tilted surface are shown in Figure 4.

Assuming that k in equation is proportional to the surface roughness and the fraction of wetted area, Miwa and co-workers (8) introduced an equation to describe the direct relationship between the sliding angle and the contact angle of a water droplet on a superhydrophobic surface. The results calculated on the basis of this equation agreed well with their experimental results. Roura and Fort (10) extended the work of Miwa and co-workers. They gave a physical model of contact angle hysterisis that derives the proportionality of critical drop size to the product rf and shown in which instances contact angle hysterisis can be related to the solid–liquid interaction energy. Youngblood and McCarthy (5) emphasized in their work that the contact angle hysterisis is more important in characterizing superhydrophobicity than equilibrium contact angle, and indicated that the surface roughness controls the continuity of the three-phase contact line and thus the hysterisis. They also indicated that on a superhydrophobic surface, the metastable states for the droplet are high in energy and the barriers between metastable are low. Extrand (12) derived a contact line density criterion for estimating the suspension or collapse of liquid drops on rough surfaces by balancing body and surface forces, and suggested that all of the parameters that include the height, slope and spacing of asperities, contact angles, liquid density, and surface tension, must be considered to determine the potential for a rough surface to suspend liquid drops. Recently, Marmur (14) proposed a model system that resembles the lotus leaf surface, and concluded that nature employs metastable states in the heterogeneous wetting regime as the key to superhydrophobicity on lotus leaves. He further explained that the metastable states make the

superhydrophobicity less sensitive to the steepness and distance of the protrusions on lotus leaves.

5. Adhesion of Dust on Lotus Effect Surface and Self-Cleaning

In order to fully understand the detailed mechanism of self-cleaning, a fundamental study on the wetting property and the adhesion of particles to the lotus effect surfaces is required.

Compared with superhydrophobicity of the lotus effect, the mechanism of self-cleaning is seldom studied. In fact, in his original work, Barthlott and Neinhuis (1) indicated that the self-cleaning can be achieved if two conditions can be met: (1) the surface is superhydrophobic so that water drops have very large contact angle and small sliding angle, and (2) the adhesion between the water drop and dust particles is greater than the adhesion between the surface and dust particles. Adhesion of two components, such as adhesion of dust or dirt to a surface, is generally the result of surface-energy-related parameters representing the interaction of the two surfaces which are in contact. In general, the two contacted components attempt to reduce their free surface energy. Strong adhesion is characterized by a large reduction in free surface energy of the adhered surfaces. On the other hand, if the reduction in surface free energy between two components is intrinsically very low, it can generally be assumed that weak adhesion exists between the two components. Thus, a reduction in free surface energy characterizes the strength of adhesion. Usually dust particles consist of materials having higher surface energy than the surface materials. They are generally larger than the surface microstructure and contact only with the tips of these microstructures. This reduced contact area minimizes the adhesion between lotus leaf surface and the dust particles, so the particles can be picked up and removed from the leaf surface by a water droplet. Therefore on a lotus leaf, hydrophobic particles are less likely be removed by water droplet than hydrophilic dust particles, and small particles, which have a size close to or even smaller than the microstructures, will be pinched in the microstructures instead of being removed by water droplet.

To investigate the self-cleaning property of a lotus effect surface, the understanding of the surface chemistry and morphology's effect on the particle adhesion is critical. Therefore, it is necessary to discuss some microscale contact theories and utilize them in studying the adhesion between particles and lotus effect surfaces.

On a microscale, the resistance to contact offered by a rough surface is larger than that of a smooth surface. The roughness-induced asperity contact and deformation reduce the intensity of adhesion. To study the relative importance of surface roughness, a dimensionless number, termed roughness ratio, is introduced as follows (97):

$$\Xi = \frac{\delta}{L} \tag{7}$$

where δ is the characteristic dimension of the asperities on the rough surface and L is the characteristic dimension of a microstructure contacting the asperities, which can be considered to be the radius of curvature of the asperity R, or, alternatively, as the correlation distance between asperities.

A dimensionless number, termed adhesion parameter Θ, can be employed to study the effect of surface roughness (97)

$$\Theta = \frac{E^*}{W_a}\sqrt{\frac{\sigma^3}{R}} \tag{8}$$

where E^* is the equivalent Young's modulus, R is the radius of curvature of the asperity tips, and $W_a = \gamma_1 + \gamma_2 - \gamma_{12}$ is the work of adhesion, with γ_1 and γ_2 being the surface energies of the two surfaces, and γ_{12} being the interfacial energy. The adhesion parameter represents the statistical average of the competition between the compressive forces exerted by the higher asperities, which tend to separate the surface and the adhesion between the lower asperities.

A dimensionless number, peel number N_P (98), can be utilized to study the adhesion of dust particles to the surface microstructures. The *peel number* is the ratio of elastic strain energy stored in the deformed microstructure to the work of adhesion between the microstructure and the substrate. When $N_P > 1$, the restored elastic strain energy is greater than the work of adhesion and the microstructure will not adhere to the substrate. On the other hand, when $N_P < 1$, the deformed microstructure does not have enough energy to overcome the adhesion between the particles and the surface. When a microstructure is adhered to a rough surface, the corresponding peel number for particle adhesion to a rough surface is determined by (97)

$$N'_P = \frac{N_P}{f(\Theta)} \tag{9}$$

where N_P is the peel number for smooth contact, N'_P is the peel number considering the rough contact, and $f(\Theta)$ is a dimensionless roughness function reflecting the influence of surface roughness on adhesion, which decreases monotonically with the adhesion parameter Θ. Equation 9 indicates that the adhesion of a particle on a rough surface is reduced with increasing adhesion parameter, Θ.

For a regular rough surface, such as a saw-toothed surface, or a surface which consists of various posts that were produced by photolithography, the adhesion parameter Θ can be easily derived with equation (8), and the adhesion between dust particles and such a surface can be determined. If an irregular rough surface which contains asperities with the same radius of curvature R whose height obeys the Gaussian distribution, one can calculate the standard deviation of the distribution of asperity heights σ in equation (8), and calculate the adhesion parameter Θ. For the majority of lotus effect surface reported so far, especially those prepared by plasma etching, the height of the surface asperities usually does not likely obey the Gaussian distribution. A model developed by Chow (99) was used to describe the relative adhesion for rough surfaces. The asperity height distribution of real lotus surfaces, however, presents more

difficulties in the estimation of adhesion. Further study on the fundamentals of and relationship between surface roughness, surface energy, and adhesion is needed to establish a theoretical framework of superhydrophobicity.

6. Development of Lotus Effect Surfaces

Although the lotus effect was discovered in plants, it is essentially a physicochemical property rather than a biological property. Therefore, it is possible to achieve the lotus effect through mimicking the lotus surface structure. As indicated earlier, since the 1950s, many superhydrophobic surfaces have been prepared and reported in the literature. Although the surface structure of lotus leaves is around 20 μm, it has been found that a much wider range of surface roughness could be used to prepare superhydrophobic surface if the surface structure can properly trap air between the surface and water droplet. Studies on superhydrophobic surfaces are listed in Table 1 in order of the authors' name. Detailed discussions of these studies are divided into several categories based on the materials and processes.

It is well known that a superhydrophobic surface is a proper combination of micro- or nano-level surface structure and hydrophobic materials. Generally there are three processes with which to prepare such a surface:

1. *Directly creating these structures on hydrophobic surfaces*. Plasma technologies are widely utilized for the processing of polymers, such as deposition, surface treatment, and etching of thin polymer films.

   Polytetrafluoroethylene (PTFE), also known as Teflon, has outstanding properties. PTFE is nonsticky; very few solid substances can permanently adhere to a PTFE surface. It has a low coefficient of friction (the coefficient of friction of PTFE is generally in the range of 0.05 to 0.20). Coating PTFE on various surfaces, such as glass, ceramic, and metal, has become a mature industrial process. Lotus effect surfaces created by plasma etching of PTFE combine superhydrophobicity with the excellent properties of PTFE coatings and can withstand harsh environmental conditions. Radio frequency (13.65 MHz) oxygen plasma etching of PTFE was reported to prepare superhydrophobic surfaces (6,15,31).

   We have discovered that low frequency (30 KHz) oxygen plasma causes the PTFE surface to form needle-like structures with a submicron scale. The observed water contact angle increased from the original value of 113° for the untreated PTFE to 160° of PTFE treated for 25 min. In Figure 5, one can see that with increasing treatment time, the needle-like structures appeared and the void increases between the needle-like structures. Such a surface morphology entraps air bubbles and reduces the wetting area on the surface when it comes in contact with water drops, therefore increasing the surface hydrophobicity.
2. *Fabricating micro/nanostructures on substrates and then coat the substrate with hydrophobic thin layers*. The roughness can be prepared on solid surface by etching (7,27,33,35), addition of fillers (19,28,74), aligned

nanotubes and nanofibers (22–24,37,39,63,64), anode oxidation of metal surface (60,70), phase separation (29,32,42,45,48,51,52,58,61), solution–precipitation reaction in hot water (65,67,68), planting (100), deposition (7,38,77,78), material sublimation (8,43,56), and machining (3). Generally, the low surface energy materials can be introduced by using/mixing low surface energy bulk materials (20,29,31,33,49), deposition (21,25,37,40, 75), or silane coating (28,32,35,38,39,42,43,45,48,55,58,60,65,67,68,70, 77,78).

3. Lotus effect surfaces can be prepared by creating surface structures and introducing low surface energy materials simultaneously, such as plasma etching and fluorination of polybutadiene thin films (76), and low surface energy material solidification (20,49,59), and polymer deposition (21,40,75).

Lotus effect surfaces have been prepared in the author's laboratory by SF_6 reactive ion etching (RIE) fluorination of polybutadiene films. The C=C bonds on the surface can be easily activated and fluorinated. A stable porous surface with water contact angle above 160° was obtained, and a small sliding angle was also observed (Fig. 6). The SEM images of SF_6-etched polybutadiene thin films are shown in Figure 7. One can see that nanoscale surface roughness was fabricated on the surfaces after 5 min etching.

7. Properties and Application of Lotus Effect Materials

7.1. Switching between Superhydrophobicity and Superhydrophilicity. Reversible switching between superhydrophobicity and superhydrophilicity has attracted many attentions. Such a surface may be applied in functional textiles, intelligent microfluidic switching, controllable drug delivery, and thermally responsive filters (63). Sun and co-workers (64) fabricated three-dimensional anisotropic aligned carbon nanotube by chemical deposition method with well-defined structures, and indicated that the superhydrophobicity with water contact angle larger than 150° and hydrophilicity with water contact angle less than 30° can both be achieved on the surface by varying structure parameter without alteration of chemical composition. Later, they reported that the wettability of a poly(*N*-isopropylacrylamide)-modified surface can be reversibly switched between superhydrophobicity and superhydrophilicity in a narrow temperature range of about 10°C (63). Krupenkin and co-workers (35) demonstrated a dynamic electrical control of wetting behavior of liquid on nanostructured surface, and the wettability can be switched from superhydrophobicity to nearly completed wetting. Most recently, Liu and co-workers (25) prepared a superhydrophobic ZnO thin film, which exhibited hierarchical structure with nanostructures on sub-microstructures, by the Au-catalyzed chemical vapor deposition method. The water contact angle can be switched from superhydrophobic (164.3°) to a superhydrophilic one (CA $< 5°$) after uv illumination, which can be recovered by being placed in the dark or being heated.

7.2. Transparent Lotus Effect Thin Films. Since the later 1990s, people pay more attention to transparent thin films with lotus effect due to their many attractive properties (42,43,45,48). In their review paper (44), Nakajima

and co-workers indicated that transparency and surface superhydrophobicity are actually competitive properties, because surface roughness will introduce light scattering. It is also indicated that, because the visible light wavelength is 400–750 nm, the proper size of surface roughness for transparent thin film should be less that 100 nm. The roughness can be introduced by plasma deposition of fluorinated silane (77,78), sol-gel alumina plus hot water immersion (65–69), and mixing of sublimation material with silica or boehmite (42,43,45,47,48). Then, low surface energy materials, such as fluorinated silanes, are coated on the rough surface to provide a hydrophobic thin film.

7.3. Biorepellent Coating. The lotus effect plays an important role for the lotus plants in the defense against pathogens (1). Spores and conidials of pathogenic microorganisms cannot easily deposit on the lotus leaf surfaces due to the nonwettability of the surface with wax crystalloids. In addition, on water repellent surfaces, spores and conidials are deprived of the water necessary for germination. Therefore, coatings that mimic the natural lotus leaves can be an ideal and novel self-decontaminating surface with three barriers against biological agents. The first barrier is the low surface adhesion due to the superhydrophobicity, which prevents the settling of the microorganisms on the surface. The second barrier is the water repellent property that forbids the germination of the spores. The third barrier is its self-cleaning capability that allows easy removal of the microorganisms with liquid solutions. With these three barriers, lotus effect surfaces are excellent candidates for biorepellent coating against airborne spores or bacteria, and may have potentials in both civilian and military applications.

To demonstrate the self-cleaning property of the lotus effect surfaces against spores, lotus effect coated surfaces and controls were soiled with *Bacillus subtilis* spores in our laboratory. After a certain settle time, water mist precipitated the surfaces, which were mounted at an angle of 45°. The test temperature was 25°C. Figure 8 illustrates the effect of lotus effect coating on preventing spore adhesion on the surface. One can see that a significant amount of spores adhere on the control surface after test, and a negligible number of spores adhere on lotus effect surface during the test.

7.4. Prevention of Biofouling. When one realizes the ability of lotus effect surfaces to repel airborne spores or bacteria, one may be interested in using such a surface to prevent biofouling problems. However, in a liquid environment, the lotus effect does not exist, and the prevention of biofouling is dependent on the surface roughness and surface energy of the coating, as well as the size and properties of microorganisms that form a biofilm. Biofilms are complex microorganism communities formed from populations of a single microorganism or from populations of multiple species (101). The adhesion of a microorganism is the first step of biocontamination. Factors known to be involved in adhesion can be grouped into surface characteristics of the substratum and the microorganism, surface free energy and topography and environmental conditions, transfer conditions and medium composition. In order to improve the self-cleaning capability of the lotus effect surfaces, antimicrobially active substances can be incorporated onto the prepared surfaces to produce a novel biocidal lotus effect surface. Unlike conventional self-cleaning surfaces, these biocidal surfaces resist microbial colonization or contamination, thus permitting the self-cleaning

properties to be maintained over a longer period of time. It has been disclosed in several U.S. patents (102–104) that polymers with amino function groups have antimicrobial properties. *Tert*-butylaminoethyl methacrylate, a methacrylate with a secondary amino function, is commercially available and has been used in copolymerization with other acrylate monomers to form biocidal materials. In our laboratory, the polymer blend, copolymerization, and grafting copolymerization of *tert*-butylaminoethyl methacrylate and polybutadiene followed by plasma treatment were explored to produce biorepellent lotus effect surfaces.

In conclusion, lotus effect materials can be a novel approach to prevent biofouling problems, but more experimental works are needed to investigate the effects of surface structure and material surface energy on biofilm formation.

7.5. Antistiction Coating and BioMEMS. Stiction problem is one of the major factors that limit the widespread use and reliability of microelectromechanical systems (MEMS). The fundamental mechanism to prevent stiction is either increasing the surface roughness, or coating MEMS surfaces with hydrophobic materials. By nature, lotus effect coating is a good combination of rough surface and hydrophobic materials. Li and co-workers indicated the possibility to use lotus effect surface as the antistiction coating for MEMS, and investigated the relationship between surface roughness, wetting, and stiction (105,106).

Another possible application of lotus effect thin films on MEMS is protective coatings for bioMEMS and biosensors. However, due to the wide variety of materials and fabrication of lotus effect thin films, it is difficult to draw some general conclusion of their biocompatibility. Khorasni and Mirzahed (33) fabricated superhydrophobic surface by irradiating polydimethylsiloxane (PDMS) rubber with CO_2-pulsed laser and grafting by hydroxyethylmethacrylate phosphatidylcholine. They studied the *in vitro* blood compatibility of this surface, and indicated that the superhydrophobic surface reduced platelet adhesion in comparison to control surfaces.

7.6. Self-Cleaning Coating for High Voltage Insulation Materials. Contamination on the surface of exterior insulators gives rise to leakage current and even flashover. Li and co-workers (107) indicated that a superhydrophobic and self-cleaning lotus effect coating can prevent the accumulation of contaminants on the surface of the insulators which produce a conductive layer when wet, leading to an increase in leakage currents, dry band arcing, and ultimately flashover. The new coating also offers resistance to atmospheric and chemical degradation (the coated insulators remain unaffected by salt air, airborne pollutants, rain, or humidity). Lotus effect coating also exhibits high tracking resistance to reduce damage during salt storms or other severe contamination events. It can be used in applications including glass, porcelain, and composite insulators where improved surface dielectric properties are needed, line and station insulators, bushings, instrument transformers and related devices, as well as other applications requiring tracking resistance.

Besides the applications introduced above, people have proposed to apply lotus effect surfaces as non-wettable and self-cleaning coatings on marine equipment and supplies including docks, piers, buoys, drilling platforms; building materials including glass, roofing, siding, flooring, windows, texturing compounds; sanitary including toilets, sinks, bathtubs, shower curtains, swimming

pools, kitchen surfaces, equipments, and transportation including, automobiles and boats.

It should be mentioned that although many preparation methods have been reported and numerous applications have been proposed, the following problems remain for the commercialization of lotus effect materials. First, the current majority of preparation methods reported is not economical and scalable. It is ideal to apply the lotus effect coating with conventional application techniques such as spry or spin coating without further process steps of lithography or plasma etching. BASF has developed lotus effect aerosol spray that can be easily applied on various substrates.

However, the mechanical stability of the film has to be improved. Second, the delicate surface structures of lotus effect coatings are prone to environmental damages. Natural lotus leaf surfaces can overcome this problem through new growth and regeneration. The fabricated lotus effect surfaces, however, do not possess such ability. Although researchers are now working on smart materials, biomimicking the self-renewal process of lotus leaves has a long way to go.

BIBLIOGRAPHY

1. W. Barthlott and C. Neinhuis, *Planta* **202**, 1–8 (1997).
2. E. Nun, M. Oles, and B. Schleich, *Macromol. Symp.* **187**, 677–682 (2002).
3. F. E. Bartell and J. W. Shepard, *J. Phys. Chem.* **57**, 211–215 (1953).
4. R. H. Dettre and R. E. Johnson, Jr., *Adv. Chem. Series* **43**, 136–144 (1964).
5. J. Youngblood and T. J. McCarthy, *Macromolecules* **32**, 6800–6806 (1999).
6. M. Morra, E. Occhiello, and F. Garbassi, *Langmuir* **5**, 872–876 (1989).
7. W. Chen, A. Y. Fadeev, M. C. Hsieh, Di. Oener, J. Youngblood, and T. J. McCarthy, *Langmuir* **15**, 3395–3399 (1999).
8. M. Miwa, A. Nakajima, A. Fujishima, K. Hashimoto, and T. Watanabe, *Langmuir* **16**, 5754–5760 (2000).
9. D. Oner and T. J. McCarthy, *Langmuir* **16**, 7777–7782 (2000).
10. P. Roura and J. Fort, *Langmuir* **18**, 566–569 (2002).
11. N. A. Patankar, *Langmuir* **19**, 1249–1253 (2003).
12. C. W. Extrand, *Langmuir* **18**, 7991–7999 (2002).
13. A. Marmur, *Langmuir* **19**, 8343–8348 (2003).
14. A. Marmur, *Langmuir* **20**, 3517–3519 (2004).
15. H. J. Busscher, I. Stokroos, J. G. Golverdingen, and J. M. Schakenraad, *Cells Mater.* **1**, 243–247 (1991).
16. H. J. Busscher, I. Stokroos, H. C. Van der Mei, P. G. Rouxhet, and J. M. Schakenraad, *J. Adhes. Sci. Technol.* **6**, 347–356 (1992).
17. C. Cottin-Bizonne, J. Barrat, L. Bocquet, and E. Charlaix, *Nature Mater.* **2**, 237–240 (2003).
18. G. T. Dambacher, *Kunststoffe* **92**, 65–66 (2002).
19. A. Duparre, M. Flemming, J. Steinert, and K. Reihs, *Appl. Opt.* **41**, 3294–3298 (2002).
20. H. Y. Erbil, A. L. Demirel, Y. Avci, and O. Mert, *Science* **299**, 1377–1380 (2003).
21. P. Favia, G. Cicala, A. Milella, F. Palumbo, P. Rossini, and R. d'Agostino, *Surf. Coat. Technol*. 169–170, 609–612 (2003).
22. L. Feng, S. Li, Y. Li, H. Li, L. Zhang, J. Zhai, Y. Song, B. Liu, L. Jiang, and D. Zhu, *Adv. Mater.* **14**, 1857–1860 (2002).

23. L. Feng, Z. Yang, J. Zhai, Y. Song, B. Liu, Y. Ma, Z. Yang, L. Jiang, and D. Zhu, *Angew. Chem. Int. Ed. Eng.* **42**, 4217–4720 (2003).
24. L. Feng, Y. Song, J. Zhai, B. Liu, J. Xu, L. Jiang, and D. Zhu, *Angew. Chem., Int. Ed.* **42**, 800–802 (2003).
25. H. Liu, L. Feng, J. Zhai, L. Jiang, and D. Zhu, *Langmuir* **20**, 5659–5661 (2004).
26. M. Flemming, A. Hultaker, K. Reihs, and A. Duparre, *Proc. SPIE-Int. Soc. Opt. Eng.* **5250**, 56–63 (2004).
27. J. Genzer and K. Efimenko, *Science* **290**, 2130–2133 (2000).
28. Z. Gu, H. Uetsuka, K. Takahashi, R. Nakajima, H. Onishi, A. Fujishima, and O. Sato, *Angew. Chem. Int. Ed.* **42**, 894–897 (2003).
29. J. T. Han, D. H. Lee, C. Y. Ryu, and K. Cho, *J. Am. Chem. Soc.* **126**, 4796–4797 (2004).
30. R. D. Hazlett, *J. Colloid Interface Sci.* **137**, 527–533 (1990).
31. Y. Inoue, Y. Yoshimura, Y. Ikeda, and A. Kohno, *Colloids Surf. B* **19**, 257–261 (2000).
32. T. Kako, A. Nakajima, H. Irie, Z. Kato, K. Uematsu, T. Watanabe, and K. Hashimoto, *J. Mater. Sci.* **39**, 547–555 (2004).
33. M. T. Khorasani and H. Mirzadeh, *J. Appl. Polym. Sci.* **91**, 2042–2047 (2004).
34. J. Kijlstra, K. Reihs, and A. Klamt, *Colloids Surf., A Eng.* **206**, 521–529 (2002).
35. T. N. Krupenkin, J. A. Taylor, T. M. Schneider, and S. Yang, *Langmuir* **20**, 3824–3827 (2004).
36. A. Lafuma and D. Quere, *Nature Mater.* **2**, 457–460 (2003).
37. K. K. S. Lau, J. Bico, K. B. K. Teo, M. Chhowalla, G. A. J. Amaratunga, W. I. Milne, G. H. McKinley, and K. K. Gleason, *Nano Lett.* **3**, 1701–1705 (2003).
38. M. Li, J. Zhai, H. Liu, Y. Song, L. Jiang, and D. Zhu, *J. Phys. Chem. B* **107**, 9954–9957 (2003).
39. S. Li, H. Li, X. Wang, Y. Song, Y. Liu, L. Jiang, D. Zhu, *J. Phys. Chem. B* **106**, 9274–9276 (2002).
40. Y. Matsumoto and M. Ishida, *Sens. Actuators A* **83**, 179–185 (2000).
41. M. Moeller, *Chem. Ing. Tech.* **74**, 550 (2002).
42. A. Nakajima, K. Abe, K. Hashimoto, and T. Watanabe, *Thin Solid Films* **376**, 140–143 (2000).
43. A. Nakajima, A. Fujishima, K. Hashimoto, and T. Watanabe, *Adv. Mater.* **11**, 1365–1368 (1999).
44. A. Nakajima, K. Hashimoto, and T. Watanabe, *Monatsh. Chem.* **132**, 31–41 (2001).
45. A. Nakajima, K. Hashimoto, T. Watanabe, K. Takai, G. Yamauchi, and A. Fujishima, *Langmuir* **16**, 7044–7047 (2000).
46. A. Nakajima, C. Saiki, K. Hashimoto, and T. Watanabe, *J. Mater. Sci. Lett.* **20**, 1975–1977 (2001).
47. A. Nakajima, A. Fujishima, K. Hashimoto, and T. Watanabe, *Adv. Mater.* **11**, 1365–1368 (1999).
48. A. Nakajima, K. Hashimoto, T. Watanabe, K. Takai, G. Yamauchi, and A. Fujishima, *Langmuir* **16**, 7044–7047 (2000).
49. T. Onda, S. Shibuichi, N. Satoh, and K. Tsujii, *Langmuir* **12**, 2125–2127 (1996).
50. A. Otten and S. Herminghaus, *Langmuir* **20**, 2405–2408 (2004).
51. S. Pilotek and H. K. Schmidt, *J. Sol-Gel Sci. Technol.* **26**, 789–792 (2003).
52. A. V. Rao, M. M. Kulkarni, D. P. Amalnerkar, and T. Seth, *J. Non-Cryst. Solids* **330**, 187–195 (2003).
53. S. Ren, S. Yang, Y. Zhao, X. Xiao, and T. Yu, *Int. J. Nonlinear Sci. Numer. Simul.* **3**, 785–788 (2002).
54. D. Richard and D. Quere, *Europhys. Lett.* **48**, 286–291 (1999).
55. G. Sakoske, M. Baumann, L. Poth, and G. Tuenker, *Glass Researcher* **12**, 33 (2003).

56. H. Sasaki and M. Shouji, *Chem. Lett.* **27**, 293–294 (1998).
57. D. Schondelmaier, S. Cramm, R. Klingeler, J. Morenzin, Ch. Zilkens, and W. Eberhardt, *Langmuir* **18**, 6242–6245 (2002).
58. M. H. Shang, Y. Wang, S. J. Limmer, T. P. Chou, and G. Cao, *Proc. SPIE-Int. Soc. Opt. Eng.* **5224**, 70–77 (2003).
59. S. Shibuichi, T. Onda, N. Satoh, and K. Tsujii, *J. Phys. Chem.* **1000**, 19512–19517 (1996).
60. S. Shibuichi, T. Yamamoto, T. Onda, and K. Tsujii, *J. Colloid Interface Sci.* **208**, 287–294 (1998).
61. N. J. Shirtcliffe, G. McHale, M. I. Newton, and C. C. Perry, *Langmuir* **19**, 5626–5631 (2003).
62. J. Shiu, C. Kuo, P. Chen, and C. Mou, *Chem. Mater.* **16**, 561–564 (2004).
63. T. Sun, G. Wang, L. Feng, B. Liu, Y. Ma, L. Jiang, and D. Zhu, *Angew. Chem. Int. Ed.* **43**, 357–360 (2004).
64. T. Sun, G. Wang, H. Liu, L. Feng, L. Jiang, and D. Zhu, *J. Am. Chem. Soc.* **125**, 14996–14997 (2003).
65. K. Tadanaga, N. Katata, and T. Minami, *J. Am. Ceram. Soc.* **80**, 3213–3216 (1997).
66. K. Tadanaga, K. Kitamuro, A. Matsuda, and T. Minami, *J. Sol-Gel Sci. Technol.* **26**, 705–708 (2003).
67. K. Tadanaga and T. Minami, *Mater. Integ.* **13**, 69–72 (2000).
68. K. Tadanaga, J. Morinaga, A. Matsuda, and T. Minami, *Chem. Mater.* **12**, 590–592 (2000).
69. K. Tadanaga, J. Morinaga, and T. Minami, *J. Sol-Gel Sci. Technol.* **19**, 211–214 (2000).
70. M. Thieme, R. Frenzel, S. Schmidt, F. Simon, A. Henning, H. Worch, K. Lunkwitz, and D. Scharnweber, *Adv. Eng. Mat.* **3**, 691–695 (2001).
71. G. J. Toes, K. W. van Muiswinkel, W. van Oeveren, A. J. H. Suurmeijer, W. Timens, I. Stokroos, and J. J. A. M. van den Dungen, *Biomaterials* **23**, 255–262 (2001).
72. M. Wulf, A. Wehling, and O. Reis, *Macromol. Symp.* **187**, 459–467 (2002).
73. Z. Yoshimitsu, A. Nakajima, T. Watanabe, and K. Hashimoto, *Langmuir* **18**, 5818–5822 (2002).
74. L. Zhai, F. C. Cebeci, R. E. Cohen, and M. F. Rubner, *Nano Lett.* **4**, 1349–1353 (2004).
75. J. Zhang, P. France, A. Radomyselskiy, S. Datta, J. Zhao, and W. van Ooij, *J. Appl. Polym. Sci.* **88**, 1473–1481 (2003).
76. I. Woodward, W. C. E. Schofield, V. Roucoules, and J. P. S. Badyal, *Langmuir* **19**, 3432 (2003).
77. A. Hozumi and O. Takai, *Thin Solid Films* **303**, 222–225 (1997).
78. A. Hozumi and O. Takai, *Thin Solid Films* **334**, 54–59 (1998).
79. R. N. Wenzel, *J. Ind. Eng. Chem.* **28**, 988–994 (1936).
80. A. B. D. Cassie and S. Baxter, *Trans. Faraday Soc.* **40**, 546–551 (1944).
81. D. Quere, *Physica A* **313**, 32–46 (2002).
82. C. Della Volpe, D. Maniglio, M. Morra, and S. Siboni, *Colloids Surf., A* **206**, 47–67 (2002).
83. G. Palasantzas and J. T. M. de Hosson, *Acta Mater.* **49**, 3533–3538 (2001).
84. T. S. Chow, *J. Phys.: Condens. Matter* **10**, L445–L451 (1998).
85. H. Nakae, R. Inui, Y. Hirata, and H. Saito, *Acta Mater.* **46**, 2313–2318 (1998).
86. K. Topolski, D. Urban, S. Brandon, and J. De Coninck, *Phys. Rev. E: Stat. Phys., Plasmas, Fluids, and Rel. Interdisciplinary Top.* **56**, 3353–3357 (1997).
87. C. Huh and S. G. Mason, *J. Colloid Interface Sci.* **60**, 11–38 (1977).
88. G. Wolansky and A. Marmur, *Colloids Surf., A* **156**, 381–388 (1999).
89. Wolansky and A. Marmur, *Langmuir* **14**, 5292–5297 (1998).

90. J. Drelich, J. D. Miller, and R. J. Good, *J. Colloid Interface Sci.* **179**, 37–50 (1996).
91. H. Murase, K. Nanishi, H. Kogure, T. Fujibayashi, K. Tamura, and N. Haruta, *J. Appl. Polym. Sci.* **54**, 2051–2062 (1994).
92. R. E. Johnson Jr. and R. H. Dettre, *J. Phys. Chem.* **68**, 1744–1750 (1964).
93. P. S. Swain and R. Lipowsky, *Langmuir* **14**, 6772–6780 (1998).
94. J. Bico, C. Marzolin, and D. Quere, *Europhys. Lett.* **47**, 220–226 (1999).
95. C. G. L. Furmidge, *J. Colloid Sci.* **17**, 309–324 (1962).
96. J. J. Bikerman, *J. Colloid Sci.* **5**, 349–359 (1950).
97. Y.-P. Zhao, L. S. Wang, and T. X. Yu, *J. Adhes. Sci. Technol.* **17**, 519–546 (2003).
98. C. H. Mastrangelo and C. H. Hsu, *J. Microelectromech. Syst.* **2**, 44–55 (1993).
99. T. S. Chow, *Phys. Rev. Lett.* **86**, 4592 (2001).
100. Y. Kunugi, T. Nonaku, Y. B. Chong, and N. Watanabe, *J. Electroanal. Chem.* **353**, 209–215 (1993).
101. M. E. Davey and G. A. O. Toole, *Microbiol. Mol. Biol. Rev.* **64**, 847 (2000).
102. U.S. Pat. 4, 515, 910 (May 7, 1985), H. R. Rawls, A. E. Querens, and B. F. Zimmerman.
103. U.S. Pat. 6, 235, 351 (May 22, 2001), D. DiMarzio, R. G. Pirich, and J. F. Klein.
104. U.S. Pat. 5, 967, 714 (Oct. 19, 1999), P. Ottersbach.
105. J. Li, L. Fan, and C. P. Wong, in *Proceeding of the 54th Electronic Component and Technology Conference*, June 2004, Las Vegas, Nevada.
106. U.S. Pat. filed in 2003, J. Li, L. Fan, and C. P. Wong.
107. U.S. Pat. filed in 2004, J. Li, L. Fan, C. P. Wong, and F. C. Lambert.

JUN LI
ZHUQING ZHANG
JIANWEN XU
C. P. WONG
Georgia Institute of Technology

Table 1. **Processing of Superhydrophobic Surfaces**

Author[a]	Process	References
Bartell	machining paraffin surface	3
Bico	molding of silicate gel followed by F-silane coating	94
Busscher	ion etching followed by oxygen plasma of FEP-Teflon	15
Chen	plasma-polymerized HFBA, plasma-etched polypropylene spherical particles of PTFE	7
Dettre	glass bead with fluorinated wax	4
Duparre	rough oxide layers	19
Erbil	solidification of isotactic polypropylene	20
Favia	plasma deposition of fluorocarbon coatings	21
Feng	nanostructured carbon films	22,24
	aligned PVA nanofibers	23
Flemming	enhanced nanoroughness of optical thin films	25
Genzer	fabricating semi-fluorinated trichlorosilane on uv-ozone treated poly(dimethylsiloxane)	27
Gu	nanoporous silica thin film with polystyrene particles as template + fluorinated silane coating	28
Han	fabrication from a supramolecular organosilane	29
Hozumi	microwave PECVD of tetramethylsilane and fluoro-alkyl silane	77,78
Inoue	Ar-ion bombardment of PTFE	31
Kato	titania-silica coating + hydrophobic solution coating	32
Khorasani	PDMS irradiated by CO_2 pulsed laser and grafted by hydroxyethylmethacrylate phosphatidylcholine	33
Krupenkin	etching a microscopic array of cylindrical nanoposts into the surface of a silicon wafer + coating	35
Kunugi	plating of Ni and graphite–fluoride	100
Lau	coating vertically aligned carbon nanotube forest with conformal PTFE thin film	37
Li	electrochemical deposition of conductive zinc oxide thin film + fluoroalkyl silane coating	38
Li	aligned carbon nanotube + coating	39
Liu	ZnO film by Au-catalyzed chemical vapor deposition	25
Matsumoto	plasma polymerization of fluorocarbon film	40
Miwa	sublimation of aluminum acetylacetonate	8
Morra	oxygen plasma etching of PTFE	6
Nakajima	sublimation of aluminum acetylacetonate + fluoroalkyl silane coating	43
	TiO_2 thin film + fluoroalkyl silane coating	45
	phase separation of colloidal silica + fluoroalkyl silane coating	42,48
Onda	wax solidification	49,59
Pilotek	silica film by sol-gel method	51
Rao	silica aerogels based on methyltrimethoxysilane precursor	52
Ren	stearic acid adsorption on polyethyleneimine	53
Sakoske	fluoroalkyl silane coating on glass	55
Sasaki	dipping glass slides into suspension containing tetraepoxy monomer, poly(*p*-vinylphenol) and silica	56
Shang	sol-gel processing and silane coating	58
Shibuichi	anodically oxidized aluminum + fluoroalkyl silane coating	59
Shirtcliffe	sol-gel phase separation method	61

Table 1. (*Continued*)

Author[a]	Process	References
Shiu	nanosphere Lithography	62
Sun	aligned carbon nanotube film	63,64
Tadanaga	Al_2O_3 films by sol-gel method + hot water immersion + fluoroalkyl silane coating	65,67,68
Thieme	chemical modified Al surface + hydrophobic coating	70
Woodward	plasma etching and fluorination of polybutadiene film	76
Zhai	creating polyelectrolyte multilayer surface overcoated with silica nanoparticles	74
Zhang	cotton fabric coated with plasma nanoparticulate film	75

[a]All authors except for Flemming have co-authors.

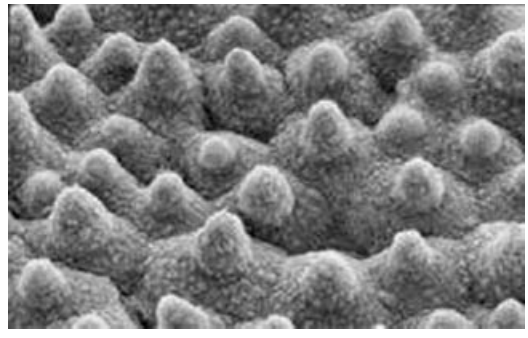

Fig. 1. Microstructure of a lotus leaf surface (1).

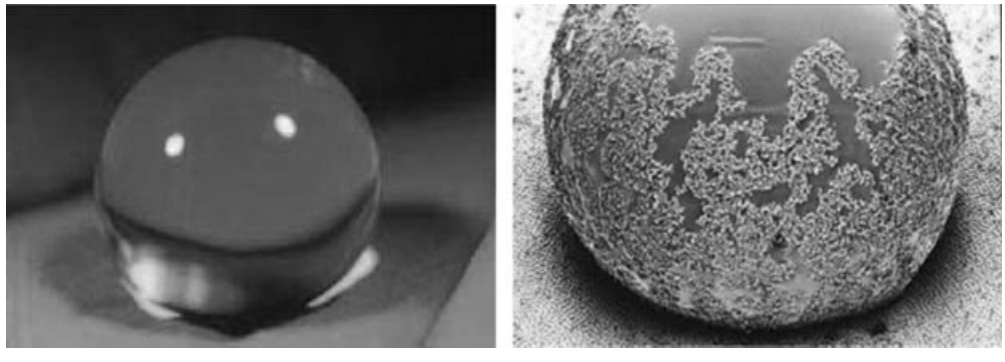

Fig. 2. Superhydrophobicity and self-cleaning property on lotus leave surface (from nanotechweb.org).

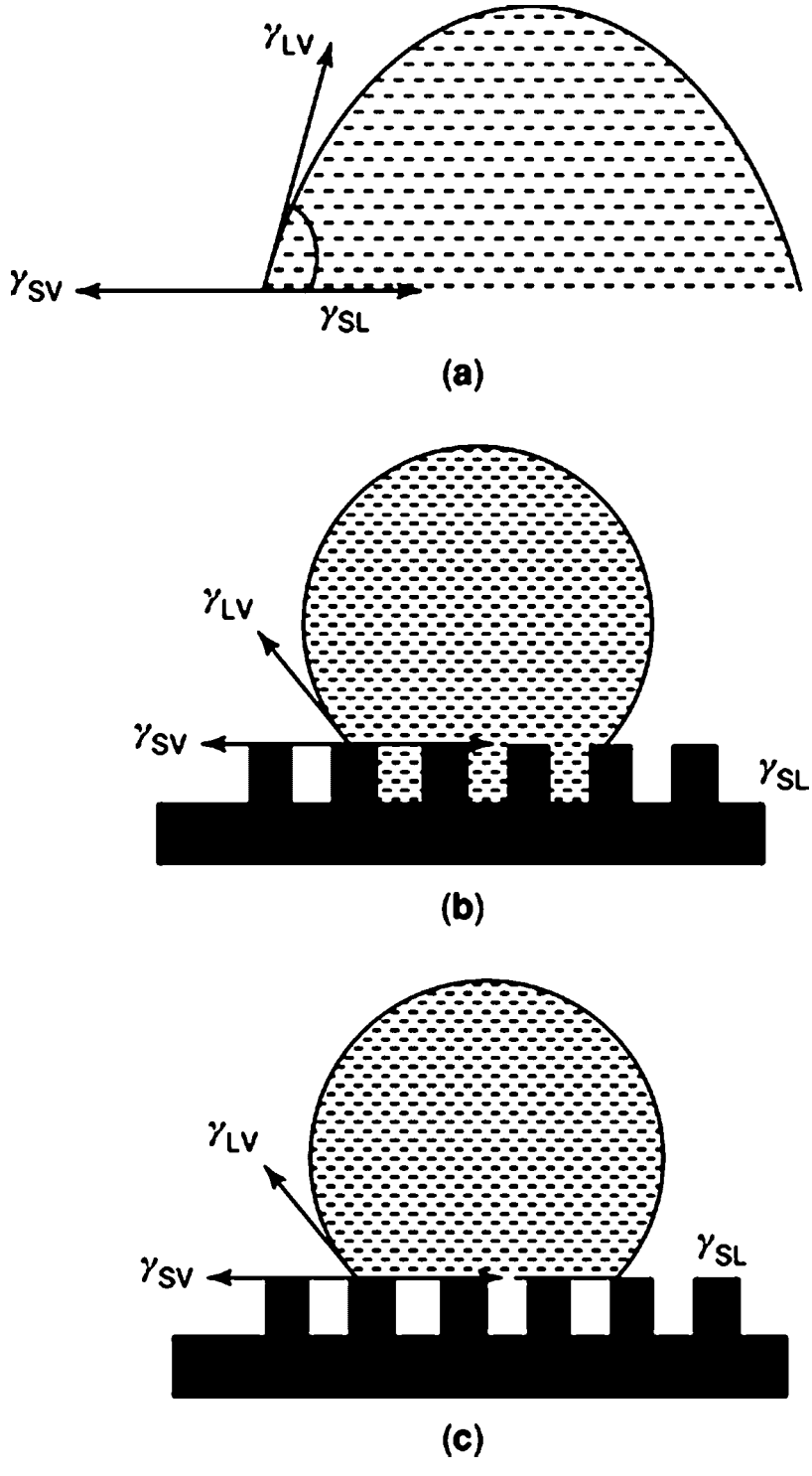

Fig. 3. Effect of surface roughness on hydrophobicity: (**a**) wetting on a flat surface, (**b**) homogeneous wetting, and (**c**) heterogeneous wetting.

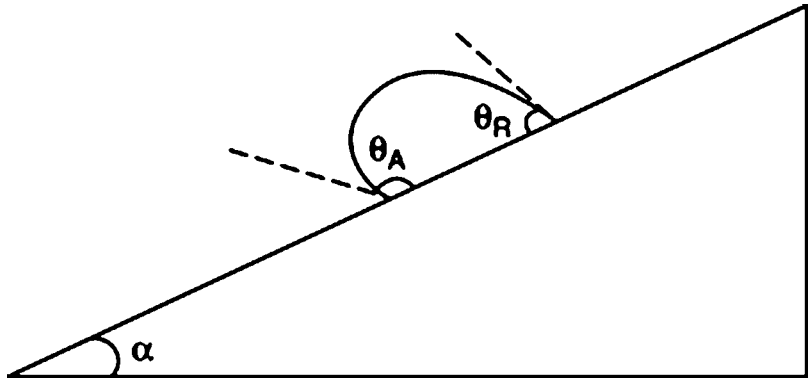

Fig. 4. Water contact angle hysterisis on tilted surface.

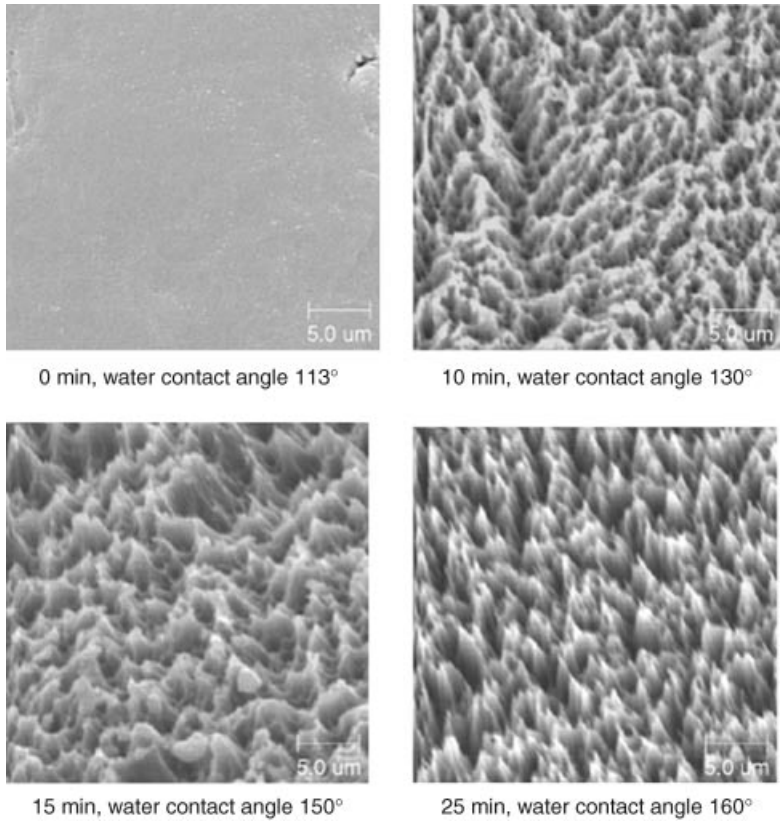

Fig. 5. SEM images of oxygen plasma etched PTFE as a function of time.

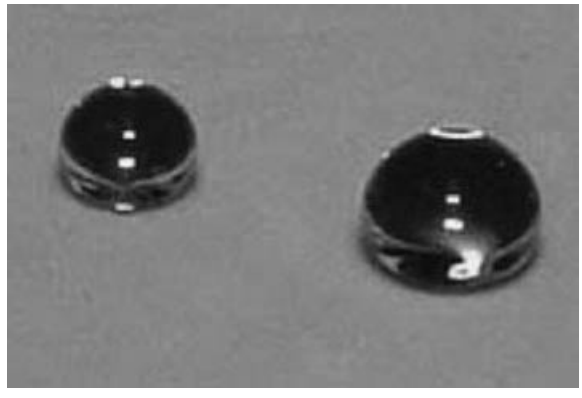

Fig. 6. Water droplet on SF_6 plasma etched polybutadiene.

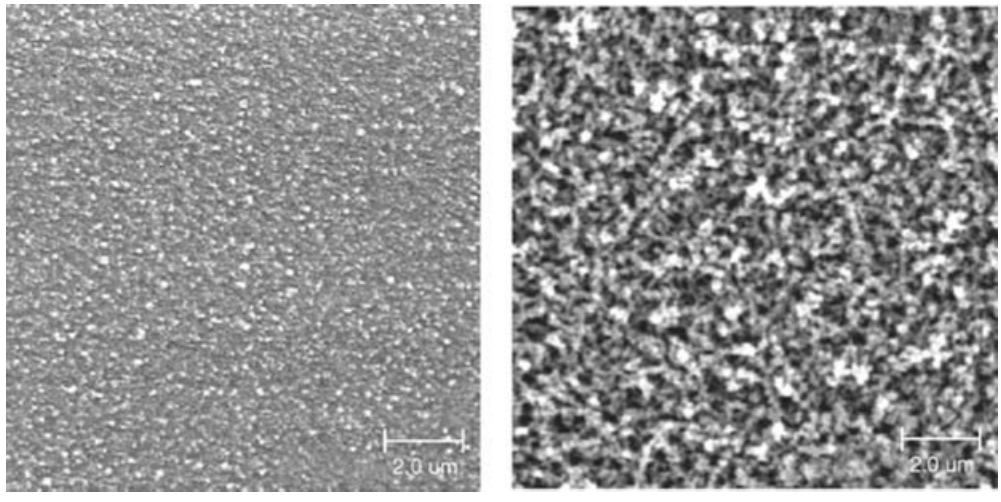

Fig. 7. SEM image of polybutadiene etched by SF_6 plasma for 1 min (left) and 5 min (right).

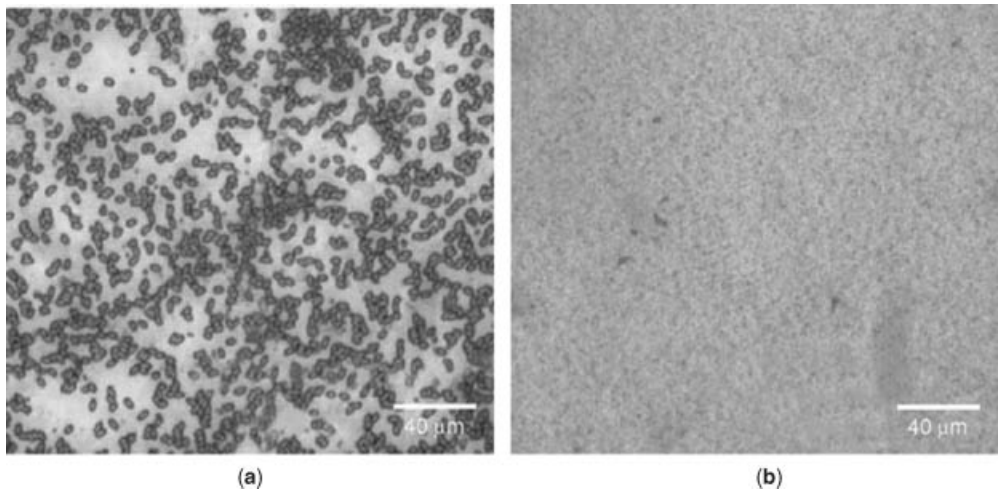

Fig. 8. Spore-repellent property of lotus effect coatings. (**a**) Control sample; (**b**) lotus effect surface.